Journal of Power Sources 192 (2009) 126–131

Contents lists available at ScienceDirect

Journal of Power Sources

journal homepage: www.elsevier.com/locate/jpowsour

Performance of solid oxide electrolysis cells based on scandia stabilised zirconia

M.A. Laguna-Bercero*, S.J. Skinner, J.A. Kilner

Department of Materials, Imperial College London, Prince Consort Road, SW7 2BP London, UK

ARTICLE INFO

Article history:
Received 14 October 2008
Received in revised form
26 December 2008
Accepted 31 December 2008
Available online 14 January 2009

Keywords:
Solid oxide steam electrolyser
Hydrogen production
Scandia stabilised zirconia

ABSTRACT

Zirconia doped with scandia and ceria (10Sc1CeSZ) is presented as an electrolyte in solid oxide electrolysis cells (SOECs) for hydrogen production at intermediate temperatures. At 700 °C, the conductivity of the 10Sc1CeSZ is 0.057 S cm^{-1} and the ohmic resistance at OCV is 0.27 Ω cm^2. The electrolysis tests using Pt electrodes show that the oxygen ion conduction in the electrolyte produces high current densities when operating as a SOEC. The performance of cells with Ni-YSZ (yttria stabilised zirconia) cathodes are also tested under external potential load at temperatures between 600 °C and 900 °C. These preliminary results demonstrate the suitability of 10Sc1CeSZ as an electrolyte for SOECs although further work is required to develop suitable electrodes.

1. Introduction

One of the major concerns in research related to future energy sources is the production and storage of hydrogen. In order to achieve zero-emission hydrogen production the hydrogen must be produced from non-hydrocarbon sources, such as the electrolysis of water [1].

At present the state-of-the-art technologies in electrolysis are low temperature alkaline and proton exchange membrane (PEM) electrolysers. The problem with these low temperature technologies is that >2/3 of the cost of electrolysis is due to electricity demand. By increasing the cell operating temperature electrical energy demand is significantly reduced [2]. In this field, solid oxide electrolysers (SOEs) offer significant power, and hence cost, savings over conventional low temperature electrolysers. Nuclear power, renewable energy and waste heat from high temperature industrial processes could be used to supply the heat and power needed for electrolysis. According to the studies of Mogensen et al. [3] SOE technology has the potential for the production of fuel from renewable energy sources or with excess energy from the primary and secondary control of existing power station capacity.

In a SOE, water is supplied to the cathode side of the cell, oxygen ions are transported to the anode through the electrolyte, and the hydrogen is produced at the cathode side. The reactions in the anode and cathode are:

$$H_2O + 2e\text{-} \rightarrow H_2(g) + O^{2-} \quad \text{(cathode)} \tag{1}$$

$$O^{2-} \rightarrow \tfrac{1}{2}O_2(g) + 2e^- \quad \text{(anode)} \tag{2}$$

Another advantage of SOEs is that they can operate reversibly as solid oxide fuel cells (SOFC) producing electricity with high efficiency by consuming the stored hydrogen. Where a fuel cell is capable of being used as an electrolyser cell it is referred to as a solid oxide regenerative fuel cell (SORFC) [2].

To date there have been relatively few investigations of ceramic electrolysers with the majority of studies focussing on the low temperature polymer based systems. Most of the ceramic electrolysers studied have been based on the high temperature yttria stabilised zirconia (YSZ) system [4,5] operating at temperatures of about 1000 °C. In order to reduce the cell operating temperature, electrolytes based on ceria have been recently studied. Zhu et al. [6] tested samarium doped ceria (SDC)-carbonate composite based SOEs and they found that both H^+ and O^{2-} transport is significant in the ceria-based composite electrolytes resulting in satisfactory electrolysis effects/processes. At 650 °C, they obtained current densities of −125 mA cm^{-2} at 1.5 V under water saturated air atmosphere.

Several efforts have been also made in order to optimise the performance of the electrodes. Wang et al. [7] tested different composite electrodes of yttria-stabilised zirconia (YSZ) with $La_{0.8}Sr_{0.2}MnO_3$ (LSM), $La_{0.8}Sr_{0.2}FeO_3$ (LSF), and $La_{0.8}Sr_{0.2}CoO_3$ (LSCo) as SOE anodes. LSF-YSZ and LSCo-YSZ composites exhibit impedances that are essentially independent of current and the same under anodic and cathodic polarization. Because LSM-YSZ composites show good performance only after cathodic activation and because this activated state is lost during operation as an SOE, LSM-based electrodes do not appear to be optimal. Marina et al. [8] also studied a wide range of electrodes. As negative electrode compositions they studied a nickel/zirconia cermet (Ni/YSZ) and lanthanum-substituted strontium titanate/ceria composite, whereas positive electrode compositions examined included mixed

* Corresponding author.
E-mail address: m.laguna-bercero@imperial.ac.uk (M.A. Laguna-Bercero).

0378-7753/$ – see front matter © 2009 Elsevier B.V. All rights reserved.
doi:10.1016/j.jpowsour.2008.12.139

ion- and electron-conducting lanthanum strontium ferrite (LSF), lanthanum strontium copper ferrite (LSCuF), lanthanum strontium cobalt ferrite (LSCoF), and lanthanum strontium manganite (LSM). They found that titanate/ceria composite electrodes seem to be more active than standard Ni/YSZ compositions for steam electrolysis. Particularly under high steam and low hydrogen partial pressures, the Ni/YSZ electrode suffered irreversible degradation. They have also demonstrated that positive electrodes generally performed less well for oxygen evolution than oxygen reduction. This behaviour was most apparent for mixed-conducting LSCuF and LSCoF electrodes, while the effect was less but still discernable for LSM. These observations are consistent with an expected decrease in the oxygen vacancy concentration as one proceeds from cathodic to anodic polarization.

Working with intermediate temperature electrolysers (500–750 °C) has potentially significant engineering advantages, such as the ease of sealing of the materials. Another advantage is the possibility of using waste heat from power stations or other industrial processes to produce hydrogen. However, the development of high-performance electrodes is essential because the electrode reaction rates at the cathode and anode decrease with lowering the temperature of operation. To this end, good performance has been reported in SOE single cells [9] and stacks [10] based on scandia stabilised zirconia (ScSZ), however, in this paper we report on the use of the electrolyte scandia stabilised zirconia substituted with ceria (10Sc1CeSZ) in a SOE, which can offer enhanced operation at intermediate temperatures.

2. Experimental

For the electrolysis measurements, 10% Sc_2O_3–1% CeO_2–ZrO_2 (10Sc1CeSZ) pellets (mol%) of 20 mm diameter and 155 ± 5 μm thickness have been used, along with Ni-YSZ (electrode)/10Sc1CeSZ (electrolyte) half-cells. Both samples were provided by Kerafol GmbH, Germany.

The phase purity of the supplied samples was confirmed with X-ray powder diffraction (XRD) using a Philips PW1700 series diffractometer with Cu Kα radiation. The XRD data were refined using the FullPROF Rietveld refinement program [11].

Scanning electron microscopy (SEM) experiments were performed under an accelerating voltage of 20 kV using a JEOL 5610LV SEM (JEOL, USA) and a JEOL 840A SEM (JEOL, USA) fitted with Oxford Instruments INCA energy dispersive analytical system (EDS) for elemental X-ray analysis. DC conductivity was measured using a 220 Keithley programmable current source and an Agilent 34401A multimeter.

For the electrolysis measurements Pt electrodes were applied using Pt paste (6082A, Metalor), deposited on both sides of the pellet which was then fired at 900 °C for 1 h. Pt wires were used for the current supply and potential probe and a Pt mesh was used at each electrode as a current collector. The sample was then attached to a zirconia tube and sealed using a glass sealant (Encapsulant 8190, DuPont). Nitrogen was used as carrier gas for the gas flow to the cathode when Pt/10Sc1CeSZ/Pt cells were used. Mixtures of hydrogen/nitrogen were required when using the Ni-YSZ/10Sc1CeSZ/Pt cells in order to avoid the oxidation of Ni to NiO. Steam was supplied to the cathode by use of a gas bubbler in water surrounded by a thermostatic bath maintained at a constant temperature for the required amount of steam. All gas lines located downstream of the humidifier were externally heated in order to prevent steam condensation. The anode side of the cell was exposed to laboratory air.

A frequency response analyser (Solartron FRA-1260) and electrochemical interface (Solartron FRA-1286) with supporting Zplot™ and CorrWare™ software were used to collect and analyse the electrochemical data. Electrochemical impedance spectroscopy (EIS) was performed using an Autolab PGSTAT30 fitted with a frequency response analyser (FRA) (Autolab, EcoChemie, Netherlands). Impedance measurements under potential load were performed in potentiostatic mode using a sinusoidal signal amplitude of 20 mV over the frequency range of 10 kHz to 0.1 Hz.

3. Results and discussion

3.1. Characterization of the 10Sc1CeSZ electrolyte

Phase purity of the 10Sc1CeSZ pellets, provided by Kerafol, was confirmed by XRD. The analysis reveals a cubic single phase of the stabilised-zirconia (space group *Fm-3m*) with a lattice parameter of $a = 5.0899(2)$ Å, in good agreement with other literature values (5.090 Å) [12]. In Fig. 1(left), we present a SEM micrograph showing the typical microstructure of the sample. The estimated relative density determined by the Archimedes method is 98.6%, and the average grain size, using the linear intercept method, is approximately 5 μm. The thickness of the electrolyte (155 μm) was also estimated from SEM images.

Total electrical conductivity of the pellets (16 mm × 8 mm × 0.155 mm) was determined using AC impedance spectroscopy for the low temperature data (up to 700 °C) and using the DC 4-point van der Pauw method [13] for higher temperatures. At temperatures above 700 °C, and due to the thickness of the electrolyte, the resistivity of the sample is comparable with those of the Pt wires of the

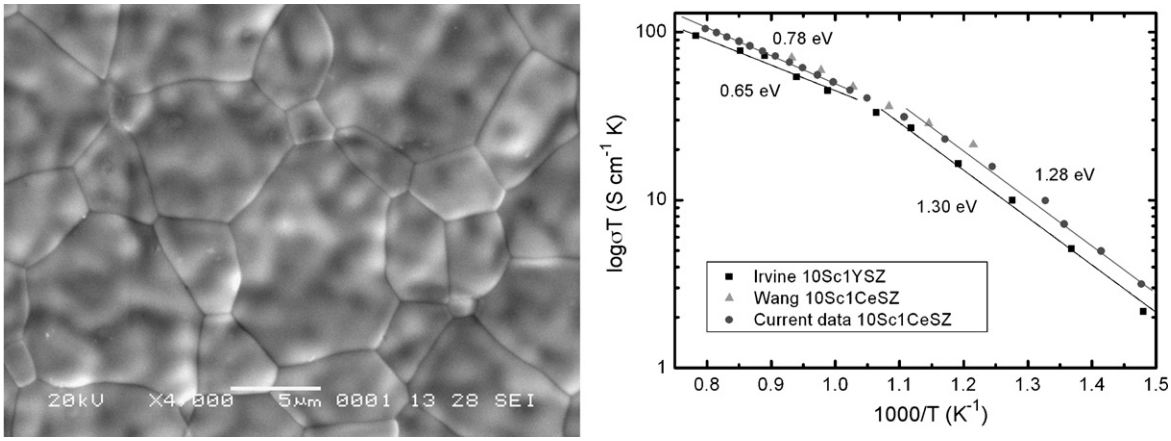

Fig. 1. (left) SEM micrograph (surface view) showing the typical microstructure of the 10Sc1CeSZ. (right) Conductivity values as a function of the temperature obtained for the 10Sc1CeSZ. Data from Ref. [14] (10Sc1YSZ) and Ref. [15] (10Sc1CeSZ) are also shown for comparison.

electrochemical rig, so it is necessary to use the DC 4-point configuration to measure the conductivity at higher temperatures. Below 700 °C, the measurements from both the DC and AC techniques are identical. In Fig. 1(right) we present the results obtained compared with the values obtained from Irvine et al. for 10% Sc_2O_3–1% Y_2O_3–ZrO_2 (10Sc1YSZ) [14] and from Wang et al. for the same composition (10Sc1CeSZ) [15]. The electrical conductivity of the 10Sc1CeSZ pellet was determined as 0.16 S cm^{-1} at 950 °C. The activation energy for the low temperature region (below 650 °C) is 1.28 eV, and for the high temperature region (above 700 °C) is 0.78 eV, which is in good agreement with other activation energy values for 10Sc1YSZ previously reported [14].

It is well known that small additions of Y_2O_3, HfO_2, CeO_2 or Ga_2O_3 stabilise the cubic phase of ScSZ at room temperature and suppress the rhombohedral phase ($Sc_2Zr_7O_{17}$) [16]. A possible mechanism of the stabilizing effect has been proposed by Arachi et al. [17]. According to their work, the larger tetravalent dopant cation was normally forming eightfold coordination with oxygen, leaving oxygen vacancies to the Zr ion which is mostly effective in stabilizing the high temperature cubic phase.

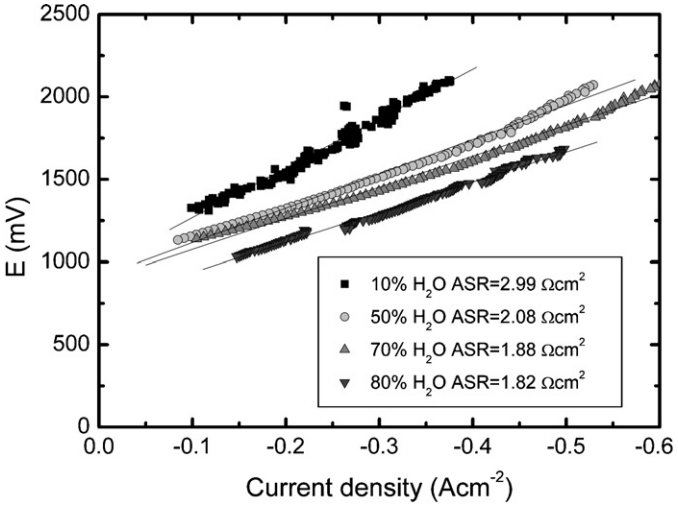

Fig. 3. Galvanodynamic experiments on a Pt/10Sc1CeSZ/Pt cell at 700 °C using N_2 as a carrier gas under different steam concentrations.

3.2. Electrolysis characterization of Pt/10Sc1CeSZ/Pt single cells

In order to determine the suitability of 10Sc1CeSZ as an electrolyte for SOE operation, we have performed several electrolysis tests using Pt as both anode and cathode. We have chosen 700 °C as the temperature of operation. At this temperature and under 3% H_2O/10% H_2/N_2 atmosphere, the conductivity of the 10Sc1CeSZ is 0.057 S cm^{-1} with an ohmic area specific resistance (ASR) for the electrolyte at open circuit voltage (OCV) of 0.27 Ω cm^2. OCVs can be predicted from the Nernst equation for any gas composition and for the reaction of the electrolysis of water, this equation can be written as

$$E = E_0 - \frac{RT}{nF} \ln \frac{P_{H_2} \sqrt{P_{O_2}}}{P_{H_2O}} \quad (3)$$

The experimental OCV obtained prior to the electrolysis test was 1.007 V, in good agreement with literature values [18]. This also indicates that there is no leakage between the sample and the zirconia tube. In Fig. 2 (left) we present a series of galvanodynamic measurements performed with a scan rate of 0.1 mA s^{-1}. Steam was supplied to the cathode side of the cell (inlet of the zirconia tube) through a gas flow saturated (nitrogen or 10% H_2/N_2 respectively) by a bubbler containing room temperature water (steam concentration about 3%), in order to examine the kinetics of Pt electrodes with respect to the oxygen partial pressures. Typical electrolysis behavior is obtained for the different carrier gases. It is of interest to note that similar slopes were observed in the figure for the voltage as a function of current density above 0.1 mA cm^{-2}. It is likely that a substantial hydrogen concentration is established, resulting in a linear increase in cell voltage as described by the Nernst equation. The clearly rapid sigmoid change of the current–potential curve under steam/nitrogen atmospheres indicates the start of water electrolysis at very low current densities, resulting in a jump in terminal voltage.

We have also studied the evolution of the voltage over the cell when applying a constant current. In this short-term experiment, the degradation after 5 h is very small and corresponds to 0.07% when applying 0.5 A cm^{-2} and 0.51% when applying 0.625 A cm^{-2}. This slight degradation is likely to be due to the polarization of the Pt air electrode, which is not optimized for SOE operation. The degradation is also observed by AC impedance, as shown in Fig. 2 (right), where we present results before and after the short-term electrolysis experiments. An increase from 2.71 to 2.99 Ω cm^2 in the polarization resistance (R_p) is observed. Alternative electrodes are in the process of being developed to address this point.

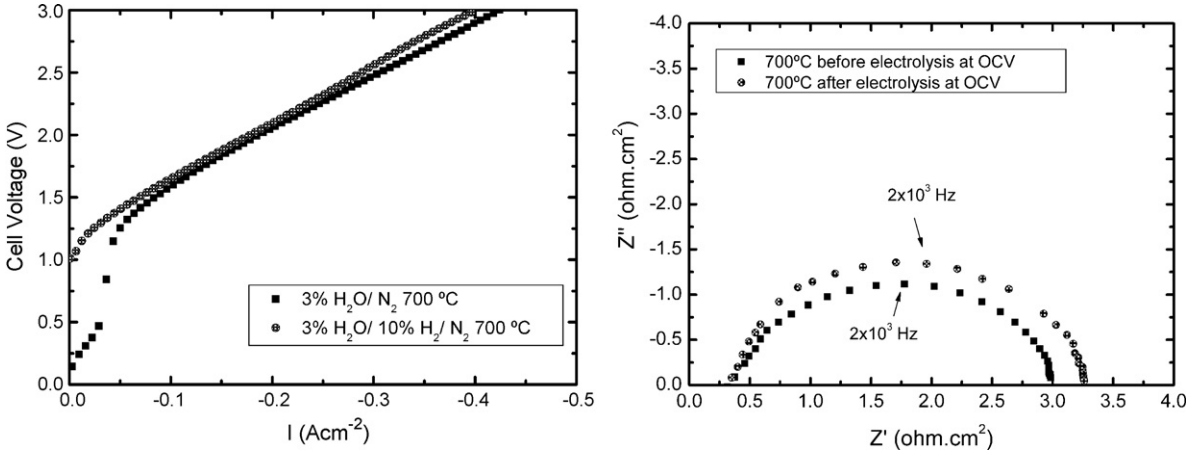

Fig. 2. (left) Electrolysis performance for an electrolyte supported cell of 10Sc1CeSZ at 700 °C. Water saturated N_2 and 10% H_2/N_2 were supplied to the cathode side and the anode was exposed to laboratory air. (right) AC impedance data for a Pt/10Sc1CeSZ/Pt cell at 700 °C measured at OCV before and after the electrolysis experiments under 3% H_2O/N_2.

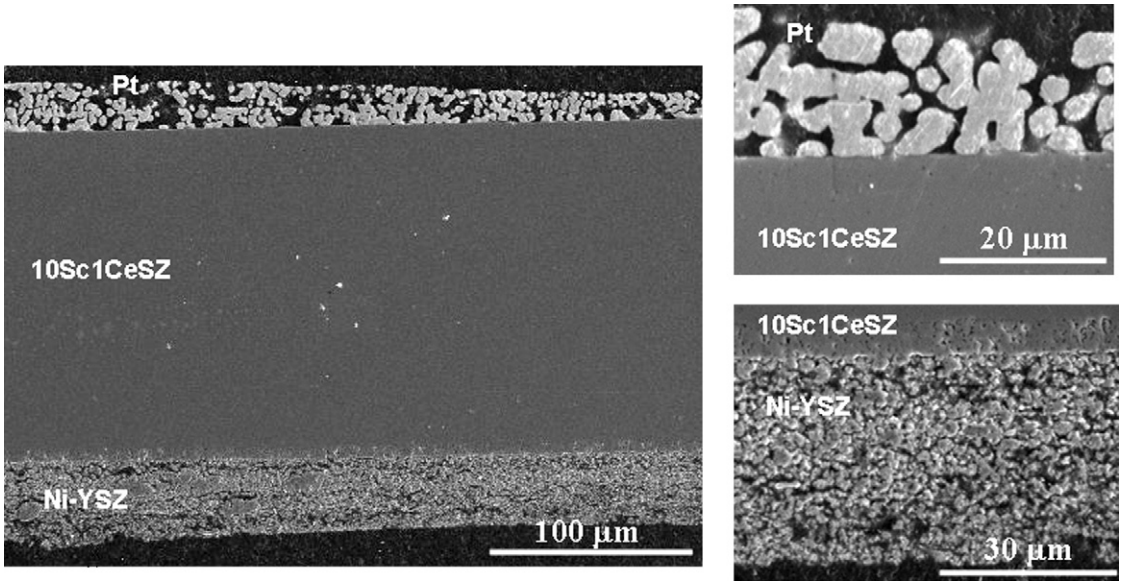

Fig. 4. SEM images (polished cross-sections) of a Ni-YSZ/10Sc1CeSZ/Pt cell.

Evaluation of the performance of 10Sc1CeSZ in electrolysis mode at higher steam concentrations is also required, as the overpotentials observed should be reduced with increasing $p[H_2O]$ [10], especially in the high current density region, probably due to an increased transfer rate of water vapor to the reaction sites [19]. In Fig. 3 we present the performance of the cell as a function of the concentration of steam introduced to the cathode side of the cell. As we increase the concentration of steam in the cathode, the performance of the cell is enhanced. In the figure we have only plotted the linear region, from which we can calculate the ASR of the cell. The best results are obtained when applying $80\%H_2O/N_2$ to the cathode side of the cell. The ASR at this concentration of steam is $1.82\,\Omega\,cm^2$. This result is slightly higher than that obtained by O'Brien et al. [18] They observed values of area-specific resistance ranging from about $0.5–1.0\,\Omega\,cm^2$, depending on test conditions using single electrolyte-supported button cells of scandia-stabilised zirconia (~175-μm thick). Note that these results were obtained at higher temperatures (800–900 °C) using strontium-doped lanthanum manganite and the nickel-zirconia cermet as electrodes. They have also observed that the degradation of ASR is associated with thermal cycling of the cells.

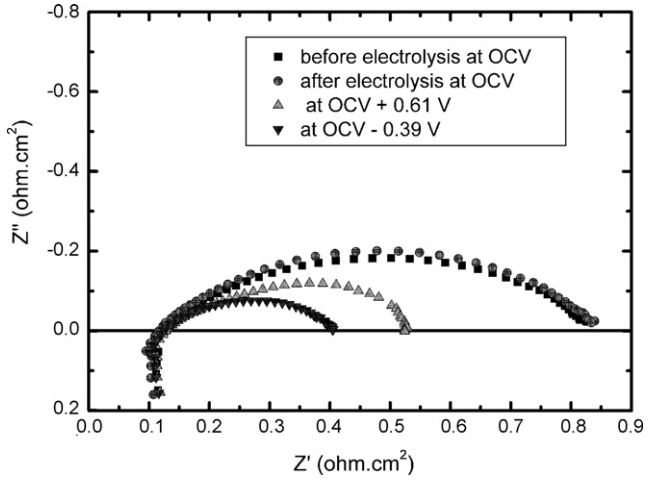

Fig. 6. AC impedance results of a Ni-YSZ/10Sc1CeSZ/Pt single cell at 900 °C measured at OCV before and after electrolysis and under different potential load.

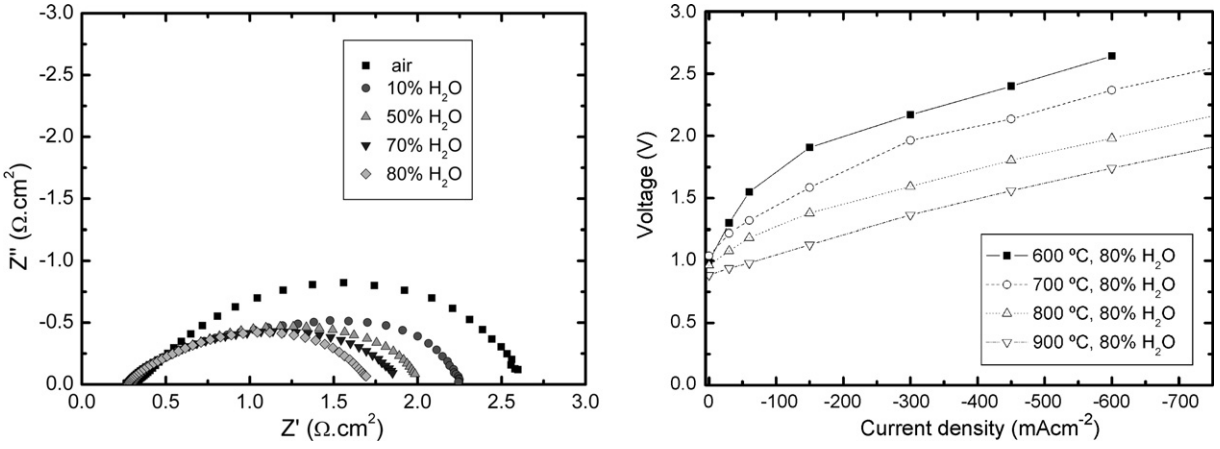

Fig. 5. (left) AC impedance results of a Ni-YSZ/10Sc1CeSZ/Pt single cell measured at 700 °C at different steam concentrations. (right) SOE experiments of Ni-YSZ/10Sc1CeSZ/Pt single cells at temperatures between 600 and 900 °C.

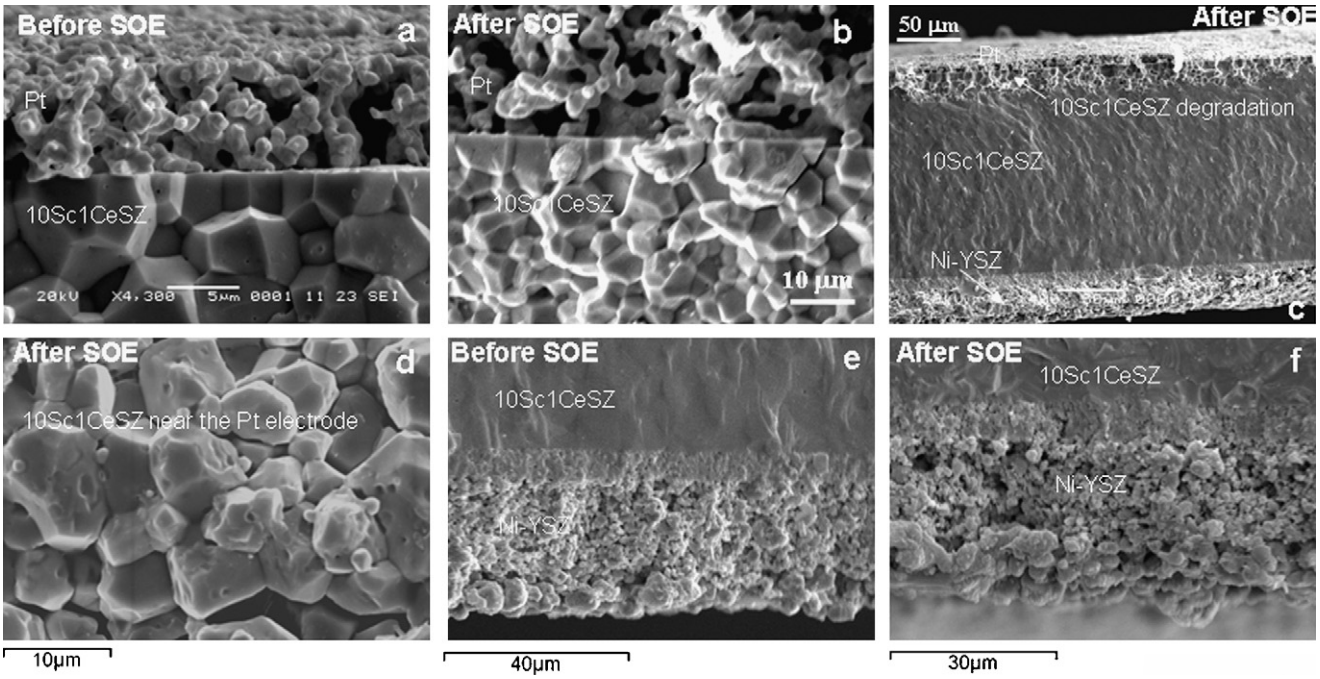

Fig. 7. Backscattered SEM images (fracture cross-section) of a Ni-YSZ/10Sc1CeSZ/Pt cell. (a) Pt/10Sc1CeSZ interface before electrolysis; (b) Pt/10Sc1CeSZ interface after electrolysis; (c) general cross-section of the Pt/10Sc1CeSZ/Ni-YSZ cell showing the 10Sc1CeSZ degradation near the Pt/10Sc1CeSZ interface; (d) 10Sc1CeSZ near the Pt/10Sc1CeSZ interface after electrolysis; (e) 10Sc1CeSZ/Ni-YSZ interface before electrolysis; and (f) 10Sc1CeSZ/Ni-YSZ interface after electrolysis.

3.3. Electrolysis characterization of Ni-YSZ/10Sc1CeSZ/Pt single cells

We have tested in SOE mode half-cells of Ni/YSZ-10Sc1CeSZ supplied by Kerafol using Pt as the oxygen electrode. Typical microstructure of a polished cross-section is shown in Fig. 4. Thicknesses of electrodes are: 40 μm (Ni-YSZ) and 20 μm (Pt). In the micrographs on the right we observe good adhesion at both electrode–electrolyte interfaces (Pt/10Sc1CeSZ and Ni-YSZ/10Sc1CeSZ).

First experiments with this sample were performed to study the electrical response of the cell as a function of the concentration of steam. H_2 (5 mL min^{-1}) and N_2 (45 mL min^{-1}) were passed through a bubbler in water surrounded by a thermostatic bath maintained at a constant temperature for the required amount of steam. The polarization resistance results (Fig. 5 (left)) clearly show a decrease in the R_p as we increase the concentration of steam supplied to the cell, obtaining best results at a steam concentration in the carrier gas of 80%, consistent with our earlier results on the Pt/10Sc1CeSZ/Pt symmetrical cell.

We have also performed SOE studies as a function of the temperature as shown in Fig. 5(right). The performance of the cell clearly improves as we increase the temperature as would be expected. ASR values obtained from the slopes of the curves at 600 °C, 700 °C, 800 °C and 900 °C are 1.67 Ω cm^2, 1.45 Ω cm^2, 1.22 Ω cm^2, and 0.99 Ω cm^2, respectively. These values improve other literature data for YSZ-based cells: 1.8 Ω cm^2 at 900 °C [4] and 2.7 Ωcm^2 at 908 °C [20], but optimization of the electrodes is required in order to approach to the best SOE based on YSZ cell found in the literature, with ASR = 0.27 Ω cm^2 at 850 °C [3].

The impedance data under different potential load is presented in Fig. 6. The ohmic resistances are about 0.11 Ω cm^2 at both OCV (0.89 V) and under external potential load as expected for 155 μm 10Sc1CeSZ electrolyte resistance, a significant improvement in comparison with standard YSZ based cells [21]. The R_p at OCV before the experiments is 0.71 Ω cm^2. When we apply a total potential of 1.5 V (we are simulating SOE conditions by applying a potential of OCV + 0.61 V), the R_p was reduced to 0.40 Ω cm^2. If we simulate SOFC conditions, applying an external potential load of OCV −0.39 V, a decrease in R_p to 0.29 Ω cm^2 was also observed. In the figure, we also present the AC impedance at OCV after both SOE and SOFC simulations. The R_p was found to increase slightly (∼3%), attaining a value of 0.73 Ω cm^2.

In Fig. 7 we present SEM images (fracture cross-sections) of Ni-YSZ/10Sc1CeSZ/Pt cells before and after the electrolysis experiments. Fig. 7a (before) and b (after) shows the 10Sc1CeSZ/Pt interface of the cell. We have observed a few cracks in the electrolyte grains near the Pt electrode after electrolysis. We do not have evidence that those cracks have not been produced during the fracture process, although we have never observed them in samples before the electrolysis experiments. In Fig. 7c we observe a general cross-section of a Ni-YSZ/10Sc1CeSZ/Pt cell after electrolysis. We can observe that 10Sc1CeSZ grains near the Pt electrode present marked interfaces, possibly due to oxygen evolution. This effect becomes more noticeable in samples exposed to longer electrolysis experiments (Fig. 7d, showing 10Sc1CeSZ near the Pt interface). The poor oxygen conduction of the Pt can contribute to this effect. Oxygen reacts with the platinum at the reaction sites on the interface to form oxygen-containing species, the presence of which partially blocks the oxygen-transfer reaction. Velle et al. [22] suggested that the formation of a PtO_x compound close to the interface contributes to the degradation of the electrode. This could be the reason for the small degradation observed by EIS.

Fig. 7e and f shows the Ni-YSZ/10Sc1CeSZ interface before and after electrolysis experiments, respectively. Apparently there are no significant differences in the microstructure of the cathode–electrolyte interface for these short-term experiments.

4. Conclusions

10Sc1CeSZ is a promising material for fuel cell and electrolysis applications, and showed good stability in both modes of operation. High current densities are obtained at an intermediate temperature of operation for SOE of 700 °C using Pt

electrodes on both sides. Ni-YSZ/10Sc1CeSZ/Pt single cells also present good behavior in SOE mode obtaining current densities of $-450\,mA\,cm^{-2}$ at 1.5 V at 900 °C and a value for the ASR of $0.99\,\Omega\,cm^2$.

Considerable work will be required to develop the ScSZ based electrolyser to a position where it will be competitive with the YSZ based cells. Further work will focus on developing suitable oxygen electrodes, such as LSM (strontium-doped lanthanum manganite), LSCF (lanthanum strontium cobalt ferrite) or $La_2NiO_{4+\delta}$.

Acknowledgements

The authors would like to thank UKERC for the funding of the project and Kerafol for providing the samples.

References

[1] E. Erdle, et al., Proceedings of the Third International Workshop, vol. 2, Konstanz, Federal Republic of Germany, 1986, pp. 727–736.
[2] K.R. Sridhar, J. McElroy, F. Mitlitsky, V. Venkataraman, Solid Oxide Fuel Cells IX (SOFC-IX), vol. 1, Cells, Stacks and Systems (2005) 295, ECS.
[3] M. Mogensen, S.H. Jensen, A. Hauch, I. Chorkendorff, T. Jacobsen, 7th Solid Oxide Fuel Cell Forum Proceedings, Lucerne, Switzerland, 2006, p. P0301.
[4] K. Eguchi, T. Hatagishi, H. Arari, Solid State Ionics 86–88 (1996) 1245–1249.
[5] A. Hauch, S.H. Jensen, S. Ramousse, M. Mogensen, J. Electrochem. Soc. 153 (9) (2006) A1741–A1747.
[6] B. Zhu, I. Albinsson, C. Andersson, K. Borsand, M. Nilsson, B.-E. Mellander, Electrochem. Commun. 8 (2006) 495–498.
[7] W. Wang, Y. Huang, S. Jung, J.M. Vohs, R.J. Gorte, J. Electrochem. Soc. 153 (11) (2006) A2066–A2070.
[8] O.A. Marina, L.R. Pederson, M.C. Williams, G.W. Coffey, K.D. Meinhardt, C.D. Nguyen, E.C. Thomsen, J. Electrochem. Soc. 154 (5) (2007) B452–B459.
[9] N. Osada, H. Uchida, M. Watanabe, J. Electrochem. Soc. 153 (5) (2006) A816–A820.
[10] J.E. O'Brien, C.M. Stoots, J.S. Herring, J. Hartvigsen, J. Fuel Cell Sci. Technol. 3 (2006) 213–219.
[11] J. Rodriguez-Carvajal, Abstracts of the Satellite Meeting on Powder Diffraction of the XV Congress of the IUCr, Toulouse, France, 1990, p. 127.
[12] H. Fujimori, M. Yashima, M. Kakihana, M. Yoshimura, J. Am. Ceram. Soc. 81 (11) (1998) 2885–2893.
[13] L.J. van der Pauw, Philips Res. Rep. 13 (1958) 1–9.
[14] J.T.S. Irvine, J.W.L. Dobson, T. Politova, S. García Martín, A. Shenouda, Faraday Discuss. 134 (2007) 41–49.
[15] Z. Wang, M. Cheng, Z. Bi, Y. Dong, H. Zhang, J. Zhang, Z. Feng, C. Li, Mater. Lett. 59 (2005) 2579–2582.
[16] T.I. Politova, J.T.S. Irvine, Solid State Ionics 168 (2004) 153–165.
[17] Y. Arachi, T. Asai, O. Yamamoto, Y. Takeda, N. Imanishi, K. Kawate, C. Tamakoshi, J. Electrochem. Soc. 148 (2001) A520–A523.
[18] J.E. O'Brien, C.M. Stoots, J.S. Herring, P.A. Lessing, J.J. Hartvigsen, S. Elangovan, J. Fuel Cell Sci. Technol. 2 (2005) 156–163.
[19] H. Uchida, N. Osada, M. Watanabe, Electrochem. Solid-State Lett. 7 (12) (2004) A500–A502.
[20] E. Erdle, W. Dönitz, R. Schaumm, A. Koch, Int. J. Hydrogen Energy 17 (1992) 817–819.
[21] A. Weber, E. Ivers-Tiffée, J. Power Source 127 (2004) 273–283.
[22] O.J. Velle, T. Norby, P. Kofstad, Solid State Ionics 47 (1991) 161–167.